TRIUMF

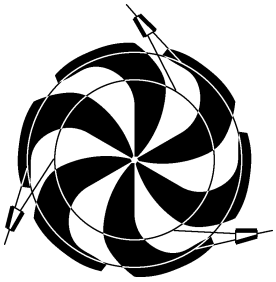

ANNUAL REPORT
SCIENTIFIC ACTIVITIES
2004

ISSN 1492-417X

CANADA'S NATIONAL LABORATORY FOR PARTICLE AND NUCLEAR PHYSICS

OPERATED AS A JOINT VENTURE

MEMBERS:

THE UNIVERSITY OF ALBERTA
THE UNIVERSITY OF BRITISH COLUMBIA
CARLETON UNIVERSITY
SIMON FRASER UNIVERSITY
THE UNIVERSITY OF TORONTO
THE UNIVERSITY OF VICTORIA

ASSOCIATE MEMBERS:

THE UNIVERSITY OF GUELPH
THE UNIVERSITY OF MANITOBA
McMASTER UNIVERSITY
L'UNIVERSITÉ DE MONTRÉAL
QUEEN'S UNIVERSITY
THE UNIVERSITY OF REGINA
SAINT MARY'S UNIVERSITY

UNDER A CONTRIBUTION FROM THE
NATIONAL RESEARCH COUNCIL OF CANADA

OCTOBER 2005

The contributions on individual experiments in this report are outlines intended to demonstrate the extent of scientific activity at TRIUMF during the past year. The outlines are not publications and often contain preliminary results not intended, or not yet ready, for publication. Material from these reports should not be reproduced or quoted without permission from the authors.

LIFE SCIENCES

Experiment LS0
PET facilities
(K.R. Buckley, TRIUMF)

The PET facilities comprise the TR13 13 MeV H^- cyclotron, the ECAT 953B/31, HRRT, and microPET tomographs, and ancillary equipment such as counting and data acquisition systems. The HRRT (high resolution research tomograph) has been used for some primate studies over the past year. The patient bed was installed in the spring. The microPET scanner has been used routinely for the past year. The ECAT 953B continues to be the most used scanner despite its advancing age though the number of scans did decrease this year. The TR13 cyclotron continues to reliably produce radioisotopes for the varied projects undertaken by the Life Sciences program.

Personnel

Caroline Williams returned from maternity leave this fall. Due to limited funding from CIHR she is working reduced hours and Shilpa Shah, who had replaced Caroline during her maternity leave, is currently available on an hourly basis.

Siobhan McCormick of the Pacific Parkinsons Research Centre has taken over the routine operation of the microPET scanner to provide consistent scanning support to the varied groups making use of this scanner.

Rabbit line

This fall a new rabbit system controller was installed to replace the old controller that had shown some anomalous errors. Incorporated in this new controller, constructed by the TRIUMF Controls group, are new sensors installed in the 9 manholes between TRIUMF and the hospital. These sensors replace the old method of passive counting of pulses from parallel coils placed around the transfer line (the rabbits have magnets inside) with active sensors that send out a digital id when the rabbit passes. This method allows for better tracking of the rabbit even when a sensor fails since it is known which sensor detected the rabbit. In the old system if one sensor was not detected subsequent sensors were misidentified. The active sensors are constructed of robust parts that (we trust) will operate for many years.

TR13 cyclotron

Usage of the TR13 cyclotron was stable this year in delivered beam and the number of irradiations. The total number of runs was 942 vs. 970 in total last year and delivered beam is 454438 μA min vs. 430630 μA min total for 2003.

Unscheduled downtime this year was quite minor. The cryocompressor internal controls continue to function poorly, occasionally turning the compressor off for no reason. This is an inconvenience but does not generally cause downtime. A one-week scheduled shutdown allowed for the installation of a new controller for the rf amplifier restoring automatic operation of the amplifier after nearly 2 years without. This controller was made and installed by the TRIUMF RF group. This extended shutdown was also used to replace seals in the vacuum valve on the injection line that had begun to leak, and to service the mechanical vacuum pumps.

The target selector lid assembly on side 1 of the cyclotron required a complete overhaul in the spring to restore electrical isolation among the 4 sector collimators in front of each target. These collimator mountings gradually build up carbon deposits that need to be removed.

One extraction foil change was required through the year and only the fluoride production target was rebuilt. Four ion source filament changes have been done along with other miscellaneous service items.

At year end all eight target locations are occupied. These consist of

- one ^{18}O-O_2 gas target (aluminum body)
- one ^{18}O water target (niobium body)
- one ^{16}O water target (aluminum body)
- one N_2/H_2 gas target (niobium body)
- one experimental flow through gas target (aluminum body)
- one experimental gas target (tantalum body)
- one experimental gas target for scattering measurements
- one location used for various solid targets.

A number of irradiations took place this year in support of LS8, in particular the production of ^{64}Cu for Oceanography. Similar beam to last year was delivered to LS4 in support of target development.

ECAT tomograph

Gantry electronics have been the dominant failures for the camera this year. In the past years replacement of some programmable logic chips in the buckets was sufficient to fix this problem. This past year some errors persisted in some boards even after changing these chips necessitating replacement of these boards. At the beginning of this year CTI gave notice that the supply of ECAT 953 and 951 parts would be discontinued at the end of March, 2004. A significant discount on an assortment of parts for the gantry electronics was negotiated, including 6 position/energy boards that have been the most failure prone item

lately. These parts were all installed in the gantry by the fall. Over the summer we received notice from the Hammersmith PET group that they were decommissioning their ECAT 953B and would sell parts to us. We have placed an order for an assortment of parts and are anxiously awaiting delivery. With receipt of these parts we hope to be able to assemble a test stand to troubleshoot a growing assortment of malfunctioning boards.

We are routinely repairing blocks in-house but have replaced only 1 block this year.

High resolution research tomograph

We are still learning our way around the HRRT scanner and interacting extensively with both CTI and other HRRT users to bring this system into routine use. The scanner has been used for some preliminary investigations with non-human primates. With the very large number of detectors in this camera (120000) the set-up and calibration is quite time consuming and the tools to do these tasks and evaluate the quality of the results are in their infancy (or non-existent). One concern for us and all HRRT users is the stability of the camera calibration but even in determining this we have encountered other obstacles. We experienced several failures of the acquisition disk array which resulted in losing some data for both stability measurements and normalizations. We believe this may have been caused by the combination of SCSI raid card and network card in the acquisition computer as determined by our computer system manager, Kelvin Raywood. The inconsistency of various software programs has also made evaluation of the camera difficult. In November the HRRT project manager visited for a few days and we were able to deal with several issues. The major task we began at that time was a complete detector set-up with a new lower gain on the phototubes. This lower gain appears to have resulted in much better position profiles but the process of the set-up for all 120000 detectors is tedious, taking 3.5 weeks. Fortunately this resulted in improved camera performance.

The patient bed arrived in June and was easily installed. Some difficulties exist with the bed motion control and we are working with CTI and the bed manufacturer to resolve these. The bed was shipped with a head holder but this holder is not adequate so an outstanding item on the to do list is to design an appropriate head holder.

MicroPET

The microPET scanner was used routinely throughout the year. The major difficulty encountered was with the transmission point source behaviour and with software updates. We have been acting as a beta test site for Concorde which necessitates an investment of time to test and evaluate the software.

The point source mechanism is used in singles mode to generate the blank and transmission scans. Occasionally the reported source position was not accurate and these files were unusable. Attempts by Concorde to fix this were prolonged but an intermediate solution is in place now.

The microPET room underwent some additional modifications to add oxygen service, anesthetic gas withdrawal, and additional cooling. This has made the room much more comfortable.

In some cases microPET scans are scheduled to coincide with tracer deliveries for the ECAT scanner to minimize load on the chemists. Two scans were thus lost this year when the ECAT scans did not proceed and the production of tracer for the microPET alone was not deemed appropriate.

Statistics

Table XVII. TR13 run statistics.

	2004	2003
Total runs conducted	942	970
Total runs lost	6	18
Total beam delivered (μA min)	454438	430630
Delivered to – LS 3	310309	294090
– LS 4	63925	63279
– LS 8	78518	55636
– LS 13	0	14066
– LS 24	0	3559
– LS 56	1210	–
– LS 60	18	–
– LS 73	458	–

Table XVIII. ECAT scanning statistics.

	2004	2003
Total scans conducted	257	388
Total scans lost	64	75
Lost to – patient	31	23
– cyclotron	6	18
– chemistry	8	3
– scanner	12	20
– staff sick/away	7	11

Table XIX. HRRT scanning statistics.

	2004	2003
Total scans conducted	36	23
Total scans lost	9	2
Lost to – chemistry	1	2
– scanner	8	0

Table XX. MicroPET scanning statistics.

	2004	2003
Total scans conducted	142	66
Total scans lost	19	10
Lost to – cyclotron	1	1
– subject	12	6
– staff sick/away	0	3
– scanner	4	0
– ECAT	2	0

Experiment LS3
Synthesis of radiopharmaceuticals for positron emission tomography
(S. Jivan, A. Studenov, TRIUMF)

The PET group at TRIUMF continued to produce 2 to 3 radiopharmaceuticals on any given day despite the fact that the CIHR grant was not funded. This absence of funding resulted in the termination of two chemistry staff members.

In collaboration with TRIUMF, the BC Cancer Agency has hired two chemists to set up and routinely produce [F-18]fluorodeoxy glucose. They will use the TR13 cyclotron and PET lab space until their eventual move to the BC Cancer Agency in downtown Vancouver.

Routine production

Table XXI summarizes the total number of deliveries to UBC hospital and other facilities, and the number of development runs.

Of the 355 deliveries sent to UBC, 17% were processed for the microPET scanner only and 9% were shared with ECAT and microPET. 14% of the total were synthesized for the HRRT scanner.

^{13}N deliveries for the Botany Department at UBC were reduced but still continue on demand. An increase in development runs was due to graduate students doing target development and researching new materials for increasing production demands.

We continue to use tetrabutylammonium fluoride, a base source in most of the ^{11}C methyl iodide reactions, to enhance and stabilize yields and lower the amount of precursor used. Most precursors are made in-house by JML Biopharm Inc. except Raclopride which is donated by ASTRA ZENECA AB.

Table XXI. Total number of deliveries for 2003 and 2004.

	2003	2004
UBC	406	355
Others*	75	57
Development runs	177	226

*UBC Botany, Chemical Engineering, PETScan Centre.

New development

Two new tracers, [F-18]FHBG and [F-18]FLT, were successfully developed and routinely produced for microPET scanning. FHBG is used as a reporter probe to image expression of herpes simplex virus type-1 thymidine kinase (HSV1-tk) reporter gene and FLT is used as a marker for cell proliferation in cancer cells. Development continues in upgrading the methyliodide system and improving yields from targets.

Experiment LS4
PET targets
(T.J. Ruth, TRIUMF)

The development of targets for the production of the neutron deficient isotopes ^{18}F ($T_{1/2}$ = 109.8 min), ^{11}C ($T_{1/2}$ = 20.4 min), ^{13}N ($T_{1/2}$ = 10.0 min) and ^{15}O ($T_{1/2}$ = 2.05 min) on the TR13 has been a major task for the TRIUMF PET group during the last several years and has been supporting a number of other projects as indicated in LS8 – Radiotracers.

Progress

Status of high current $^{18}O_2$ gas target The high current target for the production of ^{18}F-fluoride from ^{18}O-O_2 is presently going through the detailed design stage. The overall internal target dimensions have been specified based on beam size and scatter, gas pressure, stopping power, and heat transfer. The raw niobium has been purchased as has the pressure transducer, ^{18}O-O_2 gas, and the cold trap vessel. The CP42 cyclotron can deliver beam down to an energy of 23 MeV. The initial concept was to irradiate at 20 MeV and, after an analysis of the target parameters required for this energy, it was decided to incorporate a degrader to bring the beam to 20 MeV. Once the detailed target drawings are complete the target will be sent out for machining. The ATG group is currently assembling a wire scanner to be placed in front of the target to allow the beam spot to be measured and controlled.

Status of heat transfer tests Gas target heat transfer is not optimized in most gas target designs nor is it readily predictable when designing a target. Various works have looked at pressure rise behaviour as a means to determine thick target conditions and some have sought an empirical relationship between pressure and power deposition. None have proven to be generally applicable over a broad range of target designs or energies. We have begun some measurements with a heating assembly that can be inserted into a gas target to deposit a known power while observing pressure rise. With these data, heat transfer properties can be measured and ultimately optimized.

^{11}C-CH_4 production

Status of methane production As reported at last year's LSPEC meeting, we discovered that niobium is a very good target chamber material for the production of ^{11}C-methane. This result was published in the Journal of Nuclear Medicine and Biology mid-year along with the observation that an equation of the form $Y = AIe^{-at} \times \mathrm{SF}$ accurately describes the ^{11}C-methane yield from the target where A and a are fitted parameters, t is the length of irradiation, I the beam current (μA) and SF is the saturation factor $(1 - e^{-\lambda t})$. This observation implies that a first order reaction competes for the ^{11}C. Since tantalum exhibits very similar properties to niobium, it is expected to provide similar methane yields. However, a gas target constructed from tantalum provided very good ^{11}C-CO_2 yields but exceptionally poor ^{11}C-CH_4 yields (see Fig. 138). It is not understood why this is.

Interaction of the proton beam with the target chamber walls

Gas targets are the most common form of target used in the production of short-lived radioisotopes for positron emission tomography (PET). Many researchers, however, have reported a non-linear relationship between radioisotope production yield and particle beam current. This lowered yield has been attributed to several factors including the scattering of beam particles into the target body walls, radioactive species becoming trapped in the target body walls, and gas density reduction due to the deposition of heat from the incident ion beam. In this study we investigate the last factor. A 13 MeV proton beam from the TRIUMF TR13 cyclotron was used to measure the energy of scattered protons in a gas target. The average proton energy reaching the target body walls was determined by measuring the ratio of radioactivity of two simultaneously produced radioisotopes in a metal foil lining the wall of the target. The relationship between the ratio of radioactivities (production of ^{63}Zn/^{65}Zn from copper foils) and proton energy was determined using a stacked foil calibration technique. These experiments were compared to theory using a Monte Carlo program (SRIM) to model the interactions of a proton beam within a gas target.

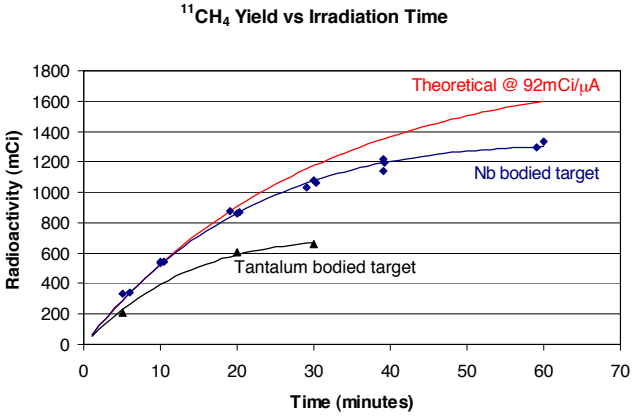

Fig. 138. Tantalum bodied target yields for ^{11}C-CO_2 ($A = 85$; $a = \mathrm{NA}$) and ^{11}C-CH_4 ($A = 41$; $a = 42$) with $I = 20\,\mu$A.

Production of ^{64}Cu

NatNi foils were irradiated with 6.9 MeV protons for the production of ^{64}Cu via the ^{64}Ni(p, n) reaction. This energy was achieved by means of an Al degrader to reduce the incident proton energy of 13 MeV to 6.9 MeV. This reduced proton energy was used to suppress the (p, α) reactions and hence the production of undesirable Co isotopes. Irradiations were nominally 4 hours with a beam intensity of 7–8 μA. After irradiation the short lived copper isotopes (^{60,61,62}Cu) were allowed to decay overnight to reduce radiation exposure to personnel. After this decay time the foils were dissolved in concentrated HCl. An AG1-X8 anion exchange column was used to separate the copper isotopes from the nickel target. The nickel was eluted with 100 ml 0.2 N HCl in 95% ethanol and the copper isotopes were eluted with 25 ml 0.1 N HCl in 75% ethanol. The solution containing the copper isotopes was evaporated and an AG1-X8 anion exchange column preconditioned with HCl was used for further purification. The remaining nickel was eluted with 25 ml concentrated HCl and the copper isotopes were eluted with 20 ml 2 N HCl. Separation using a single column was not satisfactory for this application.

Production of ^{66,68}Ga for sugar labelling

NatZn foils were irradiated with 13 MeV protons for the production of ^{66,68}Ga via the ^{66}Zn(p, n) and ^{68}Zn(p, n) reactions. Typical irradiations were 10–15 min with a beam intensity of 5 μA. After irradiation, the target foil was removed and dissolved in concentrated HCl. The gallium isotopes were extracted from this solution with isopropyl ether. The dissolved zinc target and several copper isotopes (^{61,64}Cu), which are co-produced with the gallium, remained in the acidic aqueous phase. The gallium isotopes were back-extracted with water containing a few drops of HCl. The final aqueous phase was evaporated to a few ml in volume. This production method resulted in approximately 3 mCi of ^{66}Ga and 4 mCi of ^{68}Ga two hours after the end of irradiation.

In 2004 four batches of ^{66,68}Ga were produced for sugar labelling (LS53).

Experiment LS8
Radiotracers for the physical and biological sciences
(T.J. Ruth, TRIUMF)

Many of the projects formerly associated with LS8 have been spun off into their own separate Life Sciences projects. For historical reasons, the collaboration with Botany remains the major focus of LS8 and progress in this project is reported below along with an indication of the supply of tracers for other uses within the TRIUMF community as shown in Table XXII.

Increased nitrogen uptake
(Collaboration with CELLFOR: M.Y. Siddiqi, M. Shariati, W. Li, J. Vidmar)

Our goal of increasing nitrate uptake in tobacco plants and poplar seedlings by over-expressing the high-affinity NO_3^- transporter gene (AtNRT2.1) was initially unsuccessful. Following upon our discovery that a second family of genes (the NAR2 family) must be co-expressed in order to achieve efficient NO_3^- uptake, we have successfully demonstrated that knock-out mutants of Arabidopsis lacking a functional NAR2 gene fail to absorb nitrate. We have now developed strains of tobacco over-expressing both the AtNRT2.1 gene and the AtNAR2 gene. Using $^{13}NO_3^-$ to measure nitrate uptake, we have obtained increased nitrate uptake and our preliminary growth measurements indicate increased growth in these lines. This work is now proceeding to the next stage, namely pseudo-agricultural testing in greenhouse studies being conducted by agronomists in Alberta.

$^{13}NO_3$ influx in the fungus Aspergillus nidulans: a structure function study of the NRTA gene sequence and NO_3^- uptake
(Collaboration with S. Unkles, J. Kinghorn, St. Andrews, Scotland; T. Glass, Y. Siddiqi, W. Ye, UBC)

With our Scottish collaborators, we have generated clones of Aspergillus modified at specific (putatively critical) arginine loci of the nitrate transporter protein. These arg sites are highly conserved in this gene family from fungi to higher plants. Our data have been accepted for publication in the Journal of Biological Chemistry. Replacement of arg 87 or 386 converts the protein from a high-affinity transporter with K_m's for nitrate uptake around 10 μM to a low-affinity transporter with a K_m around 15 mM. We believe that this positively charged amino acid is critical in the transmembrane uptake of nitrate. We are continuing to probe gene structure/function by replacing putative phosphorylation sites (serine and other amino acid residues) of the Aspergillus nitrate transporter. We believe that these phosphorylated amino acid residues are responsible for regulating nitrate uptake. The genetically modified fungal strains will be tested for nitrate uptake using $^{13}NO_3^-$.

Table XXII. Miscellaneous runs on the TR13 for 2004.

^{88}Y point sources for 8π group ($SrCO_3$ target)		
Date	μA min	μCi produced
June 4	61	9.2
June 11	300	117
(1 μCi and 2 μCi sources were prepared from the second run for the 8π group)		
^{48}V pins for microPET sources (Ti pin target)		
Date	μA min	μCi produced
May 26	304	5×50
June 8	35	5×11

The role of the NAR2 gene family

During his Ph.D. studies at UBC, Mamoru Okamoto isolated an Arabidopsis mutant disrupted in the NAR2 gene. We have demonstrated that this mutant is unable to grow normally when nitrate is the sole source of N and that $^{13}NO_3^-$ uptake is dramatically reduced. Thus high-affinity nitrate uptake requires the participation of both the NRT2 and the NAR2 gene families. Using molecular methods we have evidence that the two proteins are associated in the plasma membrane for normal function. This evidence (based on the yeast hybrid method) is being tested at a biochemical level by use of affinity chromatography. We have expressed the NAR2 protein in E.coli and have made an affinity resin by conjugating this protein to an immobilized cobalt affinity resin. This will be used to "fish out" the putative NRT2.1 protein. If we can successfully bind NRT2.1 to the resin via its interactions with the bound NAR2 protein, we will have strong support for the molecular evidence that the two proteins interact in the cell membrane.

Experiment LS35
Development of ^{18}F labelled nitroimidazole PET imaging agents for tissue hypoxia
(M.J. Adam, TRIUMF; D. Yapp, BCCA)

Hypoxia in cells and tissues is an important component of various pathological states (e.g. ischemia and stroke). Hypoxic tumour cells are extremely important within cancer treatment because they are more likely to survive radiation and chemotherapy, leading to an increase in tumor resistance to treatment. More recent evidence suggests that hypoxia is related to the aggressiveness of disease. Such studies employed a microelectrode, used in many centres, but were limited because of invasiveness and requirement for an accessible tumour.

Derivatives of 2-nitroimidazole are used extensively as hypoxia markers. The 2-nitroimidazoles are not metabolized in oxygenated tissues, but bind to macromolecular proteins after reduction in hypoxic cells. This permits detection by a variety of techniques. For example, the products of such binding for the (pentafluoropropyl)acetamide (EF5) and (trifluoropropyl)acetamide (EF3) derivatives of 2-nitroimidazole can be detected by specific fluorescent antibodies.

The synthesis of ^{18}F-EF5 has now been developed and was achieved by preparing the allyl precursor and fluorinating it with ^{18}F elemental fluorine in trifluoroacetic acid. The radiochemical yield is 17% after HPLC purification.

We have made considerable progress on the use of ^{18}F-EF5 as a PET tracer for imaging hypoxia in malignant tumours. The installation and commissioning of the MicroPET® scanner at the UBC hospital sparked a series of studies with animal models for cancer. The logistics involved in performing these experiments (radiotracers from TRIUMF, animals from the BC Cancer Agency, scans at the PET suite in the UBC hospital) have been resolved. We now have funding for two studies in animal tumours.

We intended to submit a clinical trial application (CTA) with Health Canada in 2004 for a pilot study to examine hypoxia in resectable lung cancer tumours. Unfortunately, this was delayed while Health Canada finalized its regulations on the human use of positron emitting radiopharmaceuticals (PERs). Thus, our original plan to carry out human PET imaging was delayed. However, Health Canada has now provided our group with guidance on the combined (labelled and unlabelled) EF5, and Dr. Laskin has taken the lead in preparing a CTA for submission. We anticipate the application will be submitted in the second quarter of 2005. In preparation for this application, all pyrogen and sterility testing has been completed and all QC and production data are available so the Quality Information Summary (QIS) portion of the CTA can be finalized.

The animal studies first described in LS35 have gone well in 2004. We have also successfully obtained funding from the Cancer Research Society to carry out studies in a colorectal cancer model (HT-29); preliminary data and scans from LS35 were used to support this application.

Experiment LS39
Positron emission profiling (PEP) for pulp and paper fluid dynamic studies

(M. Martinez, UBC)

Over the past year, we have attempted to extend the PET technique and measure the activity distribution in pulp suspension flowing in a tube with a sudden expansion in its area. Three preliminary scans have been conducted and a numerical simulation of the experiment has been developed.

Background

It is widely known that pulp suspensions do not flow until a certain critical shear stress (or yield stress) is exceeded. With traditional papermaking, the suspension is initially fluidized by turbulence created locally from a sudden change in flow area in a device called a "head box". In this case, the fibre network is broken down into smaller flocs and single fibres with weakly correlated velocities. Suspension fluidization is attained by inducing turbulence and is aided by the addition of chemical deflocculants. Characterizing this event is difficult as these suspensions are opaque.

Progress

Over the past 12 months we have built the experimental apparatus, performed three preliminary scans on the microPET, and started developing a numerical algorithm to simulate the experiment.

The flow loop used in the experiments consists of a 30 gallon tank, a 1.5 hp centrifugal pump, two magnetic flow meters, two pressure transducers, a recirculation path, and valves for control. The test section is made of clear polycarbonate and has a 2.75 in. inner diameter and is 46 in. long. The inlet diameter is 0.55 in. forming a 1:5 sudden expansion on one end and a 5:1 sudden contraction on the other. The flow reaches and leaves the test section through 15 ft. lengths of 0.55 in. inner diameter reinforced hose. Both ends of the test section are terminated with a pair of full bore ball valves and a full bore quick disconnect coupling to facilitate placement and removal of the test section into the gantry of the scanner. The test section is mounted to a 30 in. linear stage on both sides of the scanner so that the test section can be moved along its axis. To shield the scanner's detector blocks from events originating outside of the camera, 3/4 in. lead shielding is positioned concentrically with the test section up against the scanner. Three scans were conducted last year.

Experiment LS50
Antisense imaging nucleic acids for Parkinson's disease

(H. Dougan, TRIUMF)

A sizable literature exists demonstrating the antisense action of short DNA sequences on brain messenger RNAs. With the loss of such mRNAs, production of specific proteins is knocked down, leading to observable changes in animal physiology and behavior. We have a specific interest in mRNAs related to Parkinson's disease. We wish to image such mRNAs using radiotracer DNA molecules. So far, our labelled DNAs have

been unsuccessful in this application. A classical problem with pharmaceuticals is crossing the blood brain barrier (BBB), and this is probably related to our difficulties. We are currently studying two technologies for crossing the BBB. One technology is infusion of the DNA into the brain through a fine capillary. The second technical approach to the BBB problem is transport of the DNA using an antibody directed to the iron transportation mechanism in the BBB.

Experiment LS51
Auger therapy for prostate cancer
(H. Dougan, TRIUMF)

Experiment LS51 examines the possibility of killing prostate cancer cells using an iodoandrogen steroid (EMIVNT labelled with ^{125}I or ^{123}I) brought into proximity with cancer cell DNA by the androgen receptor. The graduate student M. Fedoruk believes that he made the preliminary observation that [^{125}I]EMIVNT results in small but detectable Auger killing of a line of prostate cancer cells in tissue culture. This was presented at 5ISR in Whistler, BC in September. A multidisciplinary group of scientists has formed from the BC Cancer Agency and the Prostate Centre to find the strengths and liabilities of EMIVNT for prostate cancer therapy. At present there is optimism that a drug similar to EMIVNT may be developed for practical cancer therapy.

Experiment LS53
Synthesis of ^{99m}Tc and ^{186,188}Re sugar derivatives
(M.J. Adam, TRIUMF; C. Orvig, UBC)

An NSERC strategic grant was awarded (October, 2001) (M.J. Adam, PI, $78,200/year for 3 years) to carry out research on the synthesis of technetium and rhenium labelled carbohydrates for use in nuclear medicine imaging and therapy. An extension to September 30, 2005 was granted. Dr. Adam is collaborating with Dr. Orvig in the UBC Chemistry Dept., AnorMED (M. Abrams, CEO), and MDS Nordion (Brian Abeysekera). Post doctoral fellows (Dr. Simon Bayly and Nathaniel Lim) and two graduate students (Cara Fisher and Charles Ewart) have also been working on this project for approximately three years. Cara Fisher was awarded an NSERC IPS scholarship for two years, starting in September, 2004, with MDS Nordion as the sponsoring company.

Radiolabelled carbohydrates have been of significant interest to nuclear medicine due to the success of 2-^{18}F-fluoro-2-deoxy-glucose (FDG) as an imaging agent in positron emission tomography (PET). This success has naturally raised the question of whether a single-photon emitting glucose analogue with similar properties to FDG can be developed for use with single-photon emission computed tomography (SPECT). In fact, just this year another group demonstrated that a glucosamine Tc complex does indeed get taken up into tumours. The mechanism for this uptake is as yet unknown. Because of the relatively short half life of ^{18}F (110 min) its use is limited to facilities that have an accelerator in close proximity to chemistry laboratories and medical facilities. ^{99m}Tc is the most widely used isotope in SPECT due to the fact that it is a generator produced, commercial isotope which makes it convenient to use and relatively inexpensive. It also has ideal physical properties for imaging. The drawback to this isotope is that it must be attached to the molecule via a chelate or organo-metal conjugate, which may perturb the system being studied. A SPECT analogue based on a widely available isotope such as ^{99m}Tc would make these agents available to the broader medical community. Among elements of the same series as Tc the isotopes ^{186}Re and ^{188}Re show promise in the development of therapeutic strategies. For a β^- emitting radioelement to be therapeutically useful, a half-life of between 12 hours and 5 days is preferred: moreover, for a 1 MeV β^- particle, the depth of penetration into tissue is approximately 5 mm. Furthermore, if some of the disintegrations are accompanied by 100–300 keV gamma photon, the behaviour of the radioelement can be conveniently followed by using a gamma camera. The nuclear properties of ^{186}Re and ^{188}Re are optimal for these purposes.

For the last three years we have been developing two synthetic approaches to the preparation of sugar-metal derivatives because of the known avidity of glucose to tumours. One approach forms compounds containing a Cp-M-tricarbonyl moiety (M = Tc or Re) and the other forms chelate compounds with *fac*-$[M(H_2O)_3(CO)_3]^+$ metal cores. With the first approach several ferrocenyl sugars have been synthesized. Attempts to synthesize the corresponding Cp-M-tricarbonyl products have been successful and we are now employing a single ligand transfer reaction. As a side project we have observed that several of these ferrocenyl sugar conjugates have shown cytotoxicity towards mouse lymphoma cells with IC_{50} values less than 20 μm. They are now being tested for cytotoxicity towards human breast cancer cells and are being examined for antimalarial activity. The second approach involving sugar-pendent ligands has been even more productive and we have now synthesized and characterized several new glucose and glucosamine Tc-99m and Re-186 complexes. The first of these has been published recently in Bioconjugate Chemistry [Bayly *et al.*, **15**, 923 (2004)]. These complexes with Tc and Re radionuclides were formed by using the *fac*-$[M(H_2O)_3(CO)_3]^+$ aqueous reagent originally de-

veloped by Alberto and co-workers. Since this first glucosamine compound we have synthesized several pyridinone, diamime and bipyridyl sugar chelate complexes with ^{99m}Tc and ^{186}Re and are now focusing on developing other tridentate and Cp-tricarbonyl ligand compounds. These are expected to be the most stable and thus, more likely to be better candidates as therapy and imaging agents. Several of these chelate ligands have also been complexed with positron emitting Cu-61,64 and Ga-66. Complexes with these isotopes are structurally different than the Tc or Re tricaronyl derivatives giving us a broader range of agents to evaluate. With this combination of SPECT and PET agents, coupled with the recent findings that similar agents are indeed taken up into tumours, we feel these compounds have significant potential as therapy and imaging in oncology.

Experiment LS56
Synthesis of radiolabelled nucleotides and oligonucleotides
(M.J. Adam, T. Ruth, H. Dougan, TRIUMF; D. Perrin, UBC)

This is a progress report on the development of chemistry for the F-18 labelling of oligonucleotides. One of the strategies that we are pursuing is to develop a general method to label the phosphorous atom directly with nca F-18 fluoride so that there is little structural change to the molecule. Thus, the biological activity of the oligo will be preserved. Model compound systems were developed this year to determine if P(III) and P(V) containing derivatives could be labelled with nca fluoride. We were able to successfully incorporate F-18 into both P(III) and P(V) model compounds. Another approach, undertaken by Dr. Perrin's group in UBC Chemistry, makes use of the fact that fluoride anion reacts readily with boron containing derivatives of oligonucleotides. A grant application to the CIHR to support this work was successful. An abstract to the 2004 Society of Nuclear Medicine meeting was presented and a manuscript on the P-F chemistry was submitted.

Experiment LS57
Quantitative imaging with the Concorde microPET®
(V. Sossi, UBC)

Several issues were addressed in relation to the microPET®: detector normalization, attenuation correction and scanning protocols.

Normalization

Detector normalization has been identified as one of the major contributors to image non-uniformity. A new component based normalization method in collaboration with D. Newport from CTI-Concorde has been developed and tested on phantom and rat data [Camborde *et al.*, Proc. IEEE/MIC, Rome, Italy (2004)]. During the course of this study a direct application of the measured attenuation correction factors was confirmed to be another very important source of image non-uniformity. Image uniformity was found to improve greatly if μ-map images were first segmented into air and tissue and the segmented regions were assigned pre-defined μ-values.

Attenuation correction

Presently, the attenuation correction factors are obtained using a rotating ^{68}Ge point source. These data result in an incorrect attenuation correction, because the effect of photon scatter in the transmission scan is not properly accounted for. Using simple water phantoms, we find a 50% overestimation of the reconstructed linear-attenuation coefficients for water using the reconstruction software and scatter correction (SC) currently provided by the manufacturer. Linear attenuation coefficients without the SC data are underestimated by 25%. These errors have also been found to vary with the size of the object being imaged and spatially over the extent of the object. Currently, we must segment the attenuation maps to obtain reasonable attenuation correction factors (ACFs). However, noise in the reconstructed attenuation map is a significant problem, which causes this segmentation to be difficult and highly user dependent. We are currently investigating scatter correction methods for transmission data.

We have also performed a preliminary investigation of a post-injection transmission protocol using the ^{68}Ge transmission source. It was found that the key step in this procedure was to apply segmentation to the μ-maps obtained from the post-injection transmission scan and to assign pre-defined μ values.

Dead time correction

As part of our collaboration with CTI-Concorde, we have also investigated the dead-time correction currently applied by the microPET® acquisition program. During these studies we have identified and resolved an error in this software.

Development and validation of bloodless scanning procedures and analysis

In this study we have investigated the possibility of obtaining an estimate of the BP using only 30 minutes of data [Sossi *et al.*, Proc. 5th Int. Conf. on Neuroreceptor Mapping, Vancouver (2004)].

The practical impact of this study is the fact that we will be able to perform two scans on rats with the same DTBZ delivery, since we produce DTBZ with a typical SA of 5300 Ci/mmol at end of synthesis (EOS).

Preliminary results indicate that specific activities as low as 600 Ci/mmol do not cause significant receptor occupancy.

Impact of measurement uncertainties on the determination of the DVR and BP

This work was prompted by a need to evaluate the feasibility of biological studies on the microPET®, i.e. to obtain an estimate of the expected accuracy with which parameters related to neuro-receptor studies can be determined on the microPET®. We thus investigated the effect of measurement uncertainty on the determination of the distribution volume ratio (DVR) and binding potential (BP) as estimated using the tissue input Logan (DVR_L, BP_L) and the ratio (DVR_r, BP_r) methods for two tracers, with the microPET® R4 camera. Parameter coefficients of variation (COV) were estimated from a combination of rat and phantom data. For ^{11}C-dihydrotetrabenazine the COV was 11% for the BP_L and 13.4% for the BP_r when using TACs obtained from individual regions of interest (ROIs) and segmented attenuation correction. The COVs were reduced to 7.5% (BP_L) and 8.6% (BP_r) when the striatal and cerebellar TACs were estimated as averages of 3 and 2 ROIs respectively. Results obtained for ^{11}C-methylphenidate (MP) yielded approximately 30% higher COVs. With measured attenuation correction the COVs were on average 100% higher [Sossi *et al.*, Proc. IEEE/MIC, Rome, Italy (2004); Sossi *et al.* (submitted to Phys. Med. Biol.)]. The practical impact of this study is the fact that we were able to obtain an estimate of the measurement accuracy which will guide us in the determination of the feasibility of various rat studies as well as a determination of the superiority of the segmented attenuation correction method compared to the measured one.

Experiment LS60
The physiological role of copper in marine phytoplankton
(M.T. Maldonado, UBC)

The short-lived radionuclides ^{64,67}Cu are used to investigate the physiological role of copper in Fe-limited phytoplankton. Physiological research during the last two years in our laboratory suggests that Fe-limited diatoms have a higher demand for Cu than Fe-sufficient cells, and that Cu limitation impairs their high-affinity Fe transport system. These results are the first to demonstrate Cu limitation of marine phytoplankton growth and a role for Cu in phytoplankton Fe uptake. During 2004, we have investigated the mechanistic role of Cu in high-affinity Fe transport systems in coastal and oceanic diatoms, using the radioisotope ^{64}Cu provided by TRIUMF.

Using the methods we have developed in our laboratory, we have measured rates of Fe uptake, Fe oxidation, and Fe reduction. Since the summer, we have measured intracellular levels of Cu in Fe-limited and Fe-sufficient coastal and oceanic phytoplankton using ^{64}Cu. In 2005 we hope to focus on determining Cu levels in various cellular compartments, and the kinetics of Cu transport of these microorganisms will be determined using ^{64}Cu.

During 2004, we processed a limited number of the samples we have collected to determine preliminary cellular Cu and Fe requirements of our diatom species using graphite furnace atomic absorption spectrometry (GFAAS). The samples were obtained from laboratory diatom cultures grown under various Fe and Cu levels, as well as from offshore, Fe-limited regions in the Antarctic and sub-Arctic Pacific Ocean. These data are limited, given how time consuming it is to process these samples and the high demand for these analytical instruments. However, these GFAAS data have been invaluable to validate the use of ^{64}Cu to determine intracellular Cu levels of Fe-limited marine phytoplankton.

An examination of published estimates of Cu:C ratios (based on linear relationships between dissolved Cu and PO_4^{3-} concentrations in oceanic nutriclines and Redfield ratios) in Fe-deficient waters determined that they are twice as high as those from other oceanic regions, suggesting that Cu uptake by the biota is significantly elevated in low Fe waters. This puzzling result is consistent with a physiological role of Cu in Fe acquisition. Yet, at present, no direct comparison has been made between particulate Cu:C ratios in low and high Fe waters. Our measurements of intracellular Cu concentrations, using ^{64}Cu, have allowed us to demonstrate that indeed the cellular Cu levels in low Fe cultures are elevated relative to Fe-replete cultures, and that phytoplankton in Fe-limited open ocean waters have high particulate copper values relative to those in non Fe-limited regions. A manuscript summarizing these findings will be submitted during the summer, 2005.

Experiment LS63
Non-invasive monitoring of tumour progression in the Shionogi tumour model for prostate cancer
(M.J. Adam, TRIUMF; D. Yapp, BCCA)

In the first 8 months of this project, efforts were focused on optimizing the synthesis of ^{18}F-EF5 and time for distribution of the radiolabelled tracer to obtain images with the best signal-to-noise ratios. In addition, we have also used ^{18}F-FDG (fluorodeoxyglucose) to image viable tumour tissue and thus locate the po-

sition of the tumour on the mouse image.

Mice bearing androgen dependent (AD) and androgen independent (AI) tumours have been imaged with ^{18}F-EF5 followed by ^{18}F-FDG. In a typical experiment, the animals were anesthetized (halothane), and placed on the scanning bed. ^{18}F-EF5 was injected intravenously (tail vein) and the animal was scanned, initially for 4 hours; subsequent scans were carried out 3 hours after injection of the labelled EF5 for 30 minutes. Once the EF5 scans were completed, ^{18}F-FDG was injected and the animal was re-scanned.

These experiments indicated that ∼60 μCi of ^{18}F-EF5 was appropriate for imaging tumour hypoxia in Shionogi tumours grown in DD/S mice. A similar dose for ^{18}F-FDG was also used in the same animal. The 4 hour scan was done to obtain a time-activity curve (TAC) to determine the kinetics of EF5 uptake in tumour tissue. The ratio of ^{18}F-EF5 activity between tumour and non-tumour areas was found to be as high as 1.9. Areas of uptake in AI tumours were generally more consistent and well distributed compared to AD tumours. FDG uptake was useful for delineating the edges of the tumour, differentiating between viable and necrotic areas in the tumour. No significant differences between FDG uptake in AD and AI tumours were found. Funding has been provided by a one year grant from the Prostate Cancer Research Foundation.

Experiment LS69

***In-vivo* studies on regulation of dopamine turnover using a Parkinson's disease rat model and a microPET**

(V. Sossi, UBC)

In preparation for the initiation of this study two aspects were examined: PET estimate of lesion severity and effect of anesthesia.

A key aspect of the studies described in this proposal is the determination of relative changes in vesicular monoamine transporter (VMAT2) marker ^{11}C-dihydrotetrabenzine (DTBZ) and dopamine transporter (DAT) marker ^{11}C-methylphenidate (MP) binding in rat striata. It was thus essential to determine if lesion severity could be properly assessed by PET and not be confounded by instrumental limitation such as the finite PET resolution. One of the methods to quantify lesion severity in a rat model with PET is to compare tracer binding in the lesioned side to that of the healthy side. In a preliminary study we have scanned 6 unilaterally 6-HODA lesioned rats with DTBZ and MP, and determined the BP for both striata. Subsequently we sacrificed four of the six rats and performed post-mortem [^{3}H]WIN35,428 (for DAT) and [^{11}C]DTBZ (for VMAT2) binding. The PET studies were done in identical conditions for two anesthetics: isofluorane and ketamine/xylazine. This was done to compare the effect of two anesthetics on the PET measures, since anesthesia is known to influence binding potential (BP) measures in a tracer and receptor type dependent manner.

Lesion severity was estimated as $BP_{lesion}/BP_{healthy}$ for both PET and post-mortem measures. Results are shown in Fig. 139. Excellent correlation was found between PET measures and post-mortem measures indicating that lesion severity can be accurately assessed with PET. For DTBZ the linear correlation coefficient (r^2) between the two PET estimates was 0.98 with $BP_{iso} = 1.22\ BP_{ket} + 0.1662$. r^2 between BP_{iso} (BP_{ket}) and $BP_{post-mortem}$ was 0.93 (0.91) with BP_{iso} (BP_{ket}) = 0.0077 (0.0055)$BP_{post-mortem}$ + 0.19 (0.16). For MP the r^2 between the two PET estimates was 0.92 with $BP_{iso} = 1.47\ BP_{ket} - 0.0939$. r^2 between BP_{iso} (BP_{ket}) and $BP_{post-mortem}$ was 0.99 (0.96) with BP_{iso} (BP_{ket}) = 0.16 (0.093)$BP_{post-mortem}$ + 0.036 (0.141).

We thus found that for both tracers there is an excellent linear relation between the two PET BP estimates and between PET BP and post-mortem measures. We also found that the coefficients of the linear relation are different for each tracer and anesthetic (even accounting for a different scale in the post-mortem BP assessment). Anesthesia effects thus need to be accounted for when comparing relative changes in ligand-receptor BP between different tracers. To this end we are now planning to extend this study to 10 rats.

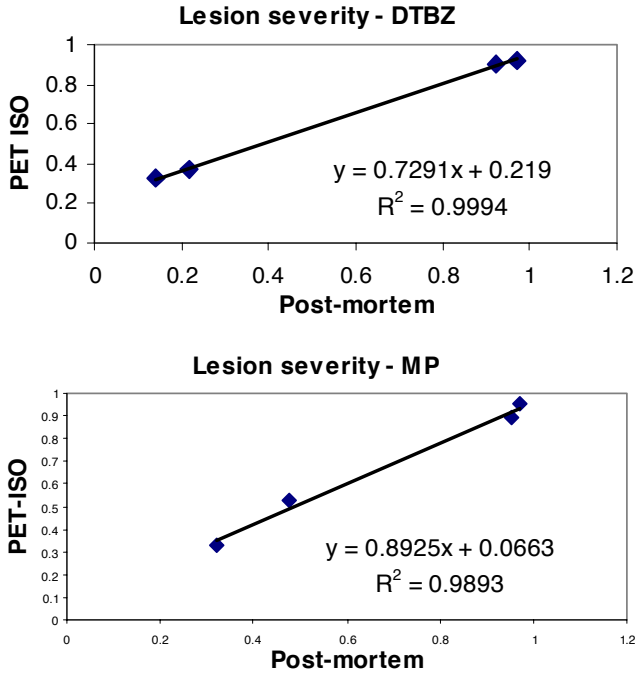

Fig. 139. Relation between lesion severity assessment with PET (under isofluorane anesthesia) and post-mortem measures for DTBZ (above) and MP (below).

These results have been submitted as an abstract to the 2005 AMI meeting [Sossi *et al.*, Proc. AMI meeting (in press)].

Most of the instrumentation and methodological advances described in LS57 will be directly applicable to the studies proposed in this research description. In particular the short scanning protocol will be used for DTBZ scans in conjunction with post-injection transmission scanning (see LS57).

Experiment LS70
Quantification of high resolution brain imaging
(V. Sossi, UBC)

Implementation of cluster and data archival system

An IBM blade server composed of 8 blades with two xenon 2.8 GHz processors and 1 MB of RAM has been installed and configured to run a parallelized version of OSEM3D (provided by CPS) under Windows. Performance tests have been done and the cluster is now ready for routine reconstructions. Likewise an automated archiving procedure has been developed.

List mode image reconstruction

The development of the list mode reconstruction was published this year [Rahmim *et al.*, Phys. Med. Biol. **49**, 4239 (2004)]. In continuation of that work we have focused on the study of convergent algorithms; i.e. iterative algorithms which (with further iterations) consistently improve such figures of merit as resolution and contrast, relevant to research and clinical tasks [Rahmim *et al.*, Proc. IEEE/MIC, Rome, Italy (2004)]. We have furthermore investigated various interpolation techniques, used in the forward- and back-projection operations in statistical list-mode reconstruction: 1) Siddon interpolation (fastest), 2) bilinear and 3) trilinear (most accurate) interpolation techniques. We have demonstrated that bilinear interpolation results in an approximately 15% improvement in resolution (2.7 mm as opposed to 3.1 mm in the centre of the field of view), while increasing the reconstruction time only by 20%.

We are currently performing final testing of the quantification accuracy of the list mode reconstruction (both the ordinary and convergent subset versions, using bilinear interpolation and a comparison of image reconstruction algorithms.

Patient motion correction

The paper describing the inclusion of motion correction into image reconstruction has been published [Rahmim *et al.*, IEEE Trans. Nucl. Sci. (in press)]. We have now acquired the Polaris^{TM} tracking system and are currently in the process of setting it up and defining its optimum position with respect to the HRRT field of view. We found that with the current marker plate the sensor was able to see the passive marker tool in the scanner at distances of 155 cm and greater, however, often only three of the four markers were visible. These experimental results agree with the calculated FOV values. We are currently investigating the possibility of building a smaller plate, which would decrease the required distance between the Polaris system and the scanner.

The current Polaris marker geometry has a maximum distance of 164.0 mm between the markers. The restrictions on the marker separation and positions are that each segment is at least 5 mm apart from all others, and that the minimum distance between markers is 50 mm. Using these guidelines, we could have a smaller tool with a maximum distance between markers of 91.2 mm thus making the use of the marker plate more practical.